An official publication of the International Society for Energy, Environment and Sustainability (ISEES)

Journal of Energy and Environmental Sustainability

Journal homepage : www.jees.in

Novel Dipstick model for Portable Bio-sensing Application

Ankur Gupta[1,#], Geeta Bhatt[2,#], Shantanu Bhattacharya[2,*]

[1]*School of Mechanical Sciences, Indian Institute of Technology Bhubaneswar, Odisha-752050, India*
[2]*Department of Mechanical Engineering, Indian Institute of Technology Kanpur-208016, India*

ARTICLE INFO

Received : 11 March 2019
Revised : 26 March 2019
Accepted : 27 April 2019

Keywords:
Nanocomposite,
Dipstick model,
Portable biosensor

ABSTRACT

In this work, we propose a novel bio-chip functionalized with hybrid nanomaterials which can provide a platform with a potential of dipstick biosensor. A ZnO-Au nanocomposite layer has been fabricated and utilized to perform FRET-based detection of *E. coli* DH5α. In solution form, FRET is always compromised due to the presence of a water-based solution and associated quenching effects. But when the FRET is carried out over films of nanoporous silica with embedded nanomaterials as synthesized in this work, there is an overall signal enhancement leading to an increase in sensitivity of the detection process. The signal enhancement is primarily due to the change in band gap energy of ZnO owing to doping through a gold layer which in turn leads to tune gap of the composite to the emission range of dye pairs. The sensitivity enhancement eventually is found to happen due to the electron cascading on gold film due to a changed band gap of the Zinc Oxide and a parallel ongoing surface-enhanced Raman scattering effect on thin gold coating causing an increased emission intensity by a few nanometres. This results in an overall enhanced signal and can lead to the detection of trace sample concentrations of microorganisms. In this way, the proposed technology can be used as an easy to use dipstick bio-sensor for microorganisms.

1. Introduction

Escalating inevitability for applications in health concerns and food safety promotes current research and development for highly target-specific sensors. There exist a range of sensing devices for DNA/bacteria which majorly depend on pre-processing steps like particle separation, particle concentration (dielectrophoresis) [Bhatt et al., 2017], polymerase chain reaction [Nayak et al., 2013], hybridization [Wang, 2005], antibody-antigen chemistry etc. There are several detection schemes to detect the obtained products and these are namely colorimetric detection[Bhatt and Bhattacharya, 2018], fluorescence-based detection [Bhattacharya et al., 2008], optical detection [Bhatt and Bhattacharya, 2018], impedance-based detection [Bhatt and Bhattacharya, 2018] and mass/cantilever based detection [Bhatt and Bhattacharya, 2018] etc. All these detection schemes demand a sophisticated microchip platform to work with. Hence the substrate plays a very significant role in sensing, as the properties of the substrate material directly influence the detection scheme. The immense progress is being made for devising the substrate to carry out the detection. In this context, substantial progress has been made from silicon technology to flexible substrates [Rim et al., 2016].

When the optical detection is carried out, surface properties directly play a significant role in detection as the obtained surface immensely influence the recorded optical characteristics. Hence the technological progress is moving in a way that the substrate is being devised in a manner that it provides more surface to volume ratio, which strongly favors the application of porous films substrates for detection purpose [Korampally et al., 2009]. The chemical etching technique has played a significant role in formulating the porous structures [Seidel, 1990]. Porous silica structure has been efficiently devised using poly (methyl silsesquioxane) using a core-shell structure where silsesquioxane acts as porogen [Su and Chen, 2009]. The nanoparticles inclusion in some form has further shown an enhancement in detection sensitivity in biosensors [Luo et al., 2006]. Various characterizations [Scandale et al., 2008, [Himcinschi et al., 2001] has been performed for optimizing the structural properties of the substrate to achieve higher sensitivity. In this context, high surface area nanostructured films and embedded metal nanoparticles within such films offer great possibilities of sensitive detection of biological entities. Of specific mention are the phenomena of Surface Enhanced Raman Scattering (SERS) which has received wide attention and audience of researchers starting from its invention in the early '70s. The basic physics behind SERS are two-fold viz., (a) the electromagnetic fields coupled to regions at or near nanoparticle surfaces, which lead to a local Surface Plasmon Resonance effect leading to an overall enhancement in the electric field (b) chemisorbed species and the metal surface being in the near vicinity of each other which may result in charge transfer processes which may ease out the energy requirements for the HOMO (high occupancy molecular orbit) to LUMO (low unoccupied molecular orbital) transitions particularly in cases where the HOMO and LUMO orbital states of the

* Corresponding Author: *bhattacs@iitk.ac.in*
# *Both authors contributed equally*

absorbents fall symmetrically about the metal nanoparticle which acts as a charge transfer intermediate. In such cases what would have otherwise necessitated much more energy (probably in UV range) may be carried out in the visible or the near infra-red spectrum [Foresman et al., 1992]. In the present work the metallic nanoparticle has an added advantage of a shortened bandgap of its core, i.e., zinc oxide (ZnO) structure which helps in quick releasing of electrons to the gold (Au) nanoparticles that may further cause an enhancement in the local plasmon wave in the Au nanoparticles and enhance the electric field in its near vicinity thus enhancing the signal intensity. Also in the current orientation, both the ZnO and Au nanoparticles are embedded within polymethylsilsesquioxane (PMSSQ) matrices where there is a good possibility for the ZnO particles to develop Zn-O-Si bonds with the matrix as has been studied earlier [Gupta et al., 2015]. The formation of the bonded HOMO-LUMO states is also inevitable when we look at the nature of the interaction between the embedment and the porous matrix.

This embedded porous structure has facilitated the immobilization of the cells onto them with great sensitivity. The various scheme can be utilized for immobilization of the biological entities on the substrate [Kant et al., 2017]. The major adsorption mechanism of the biological entities can be DNA hybridization or antibody-antigen interaction. The DNA hybridization based detection can be accomplished in case of DNA identification or sequencing while antibody-antigen bonding scheme can be utilized for protein-based detection or multiplexed profiling [Uttamchandani et al., 2009]. The principle detection scheme that we use in this work is based on antibody-antigen chemistry induced SERS fluorescence resonance energy transfer (FRET) and the final target is the detection of a micro-organism with great sensitivity and accuracy. Already the major goal of third world countries is to develop some dipstick model assisted devices which are capable of sensing micro-organisms up to an extent of 1 CFU/ mL of solution. This work shows the way forward for such a low cost and easy to use detection scheme. The other very important aspect of this process is the high porosity of the NPS film which leads to encapsulation of the analytes to a vast majority of embedment and also an elevated highly networked surface area leading to the ease of charge transfer. This dipstick model has been tested for its detection of surface proteins associated with *E. coli*DH5α and it has been found that this sensor is capable of detection of *E. coli*DH5α upto a concentration of 100 CFU/mL. This can be further optimized for the detection of 1 CFU/mLconcentration of cells with further refinements.

2. Material and Methods:

2.1 Biological Processing

For enabling the FRET to happen the monoclonal antibody labeling kit for Alexa Fluor 546 (AF546) and Alexa Fluor 594 (AF594) were purchased from Molecular Probes. Protein-G was purchased from Sigma Aldrich Pvt Ltd. P-type Si (100) substrate (from Logistics Inc., NY) was used as the platform coated with the metal embedded organic filmfor *E. coli* DH5α sensing. IPA, Acetone, methanol were all purchased from Sigma Aldrich, India.

To perform the FRET phenomenon, firstly fluorescent labeling is performed through monoclonal antibody labeling kit. All the protocols related to handling and experiments have been followed on the basis of the instructions/kits provided along with the product purchase. For antibody and protein-G conjugation, 1 M solution of sodium bicarbonate (pH ~8.3 stored at 4°C) is prepared by adding 1 mL of deionized (DI) water to the provided vial of sodium bicarbonate. The solution is properly mixed with Vortex shaker by providing up and down motion until it is completely dissolved. 1 mg/mL of antibody and protein is prepared and then the appropriate volume of 1 M and 0.1 M sodium bicarbonate buffer is added to it respectively. 100 µL of the prepared protein solution is taken to the vial of reactive dye. The vial is properly capped and gently inverted for a few times to fully dissolve the dye. The violent agitation of the protein solution can result in protein denaturation. The prepared solution is incubated for 1 hour at room temperature. After every 10–15 minutes, the vial is gently inverted several times in order to mix the two reactants and increase the labeling efficiency. In order to purify the labeled protein, the spin column is put in a 13 × 100 mm glass tube. It should be noted that the enclosed spin column should have two frits inserted at the bottom. The second or both frits are inserted into the column and pushed down to the bottom of the column. The purified resin is stirred and then 1 mL of the suspension is added into the column and is allowed to settle. More suspension is added continuously until the bed volume reaches ~1.5 mL. The column buffer is allowed to drain from the column by gravity. After this, the spin column is placed in one of the provided collection tubes and the column is centrifuged for 3 minutes at 1100 × g using a swinging bucket rotor. 100 µL reaction volume (from the previous step) is loaded dropwise onto the center of the spin column. The solution is then allowed to absorb into the gel bed. The spin column is placed into the empty collection tube and is centrifuged for 5 minutes at 1100 × g. After centrifugation, the collection tube will contain labeled protein in approximately 100 µL of PBS (pH 7.2) with 2 mM sodium azide, the free dye will remain in the column bed. After the complete process, the spin column is discarded.

2.2 Fabrication and characterization of ZnO nanoparticles

ZnO nanoparticles were synthesized with the help of Zinc acetate dehydrate, isopropanol and sodium hydroxide. Zinc acetate (0.1M) dissolved in isopropanol was mixed using the ultra-sonication process at 44 kHz till the solution dissolved completely. During mixing the NaOH solution was mixed drop by drop with the Zinc acetate solution and simultaneously the pH was maintained at 10. After proper mixing, the solution was heated to 200ºC and the dried powder was collected in a separate vial. The dried powder was centrifuged after mixing and washing was carried out with deionized water. The ZnO nanoparticles were separated by the solid-liquid separation method. The fabricated ZnO nanoparticles were characterized by Transmission Electron Microscopy (TEM) and UV visible spectroscopy (UV-vis) to confirm the presence of the nanoparticles. TEM characterization was performed on a Hitachi 8100 transmission electron microscope to determine the size and monodispersity of the resulting nanoparticle solution. For TEM, a typical sample for characterization was prepared by dropping 10 mL of nanoparticle solution onto a perforated carbon grid, followed by wicking the solution away. The grid was subsequently dried under vacuum and imaged. Figure 1 (a) and (b) show the TEM and UV-vis image, and UV-vis shows a peak at 420 nm wavelength, which is an indicator of the band gap energy in case of ZnO.

2.3 Fabrication and characterization of Gold nanoparticles

For Au nanoparticles fabrication, all glassware was oven dried after cleaning in aqua regia (3 parts HCl, 1 part HNO_3) and DI water rinsing. An aqueous solution of $HAuCl_4$ (1 mM, 500 mL) was brought to reflux while stirring, and then 50 mL of a 38.8 mM trisodium citrate solution was added quickly to it, which resulted in a change in solution color from pale yellow to deep red. After the color change, the solution was refluxed for an additional 15 min and was allowed to cool to the room temperature, and subsequently filtered through a 0.45-micron filter (Micron Separations Inc.). A typical solution of 13-15 nm diameter Au particles exhibiting a characteristic surface plasmon band centered at 518-520 nm was obtained.TEM and UV-vis characterization of the Au nanoparticles was performed to confirm the shape and size of the fabricated nanoparticles. Figure 1 (c) and (d) show the TEM and UV-vis characterization of the Au nanoparticles.

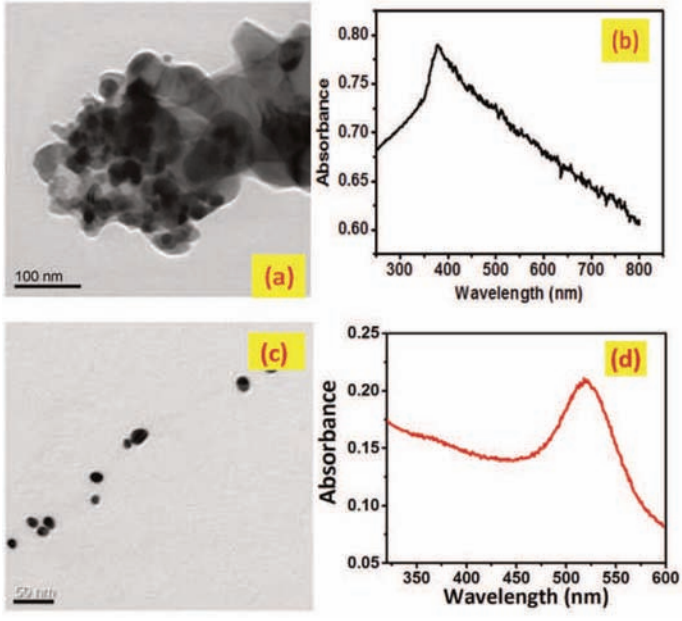

Figure 1: (a), (b) TEM image and UV-vis spectroscopy of ZnO nanoparticles; (c), (d) TEM image and UV-vis spectroscopy of Au nanoparticles

2.4 Fabrication and characterization of ZnO-Au nanocomposite and their doping in NPO structure

ZnO-Au composite has been prepared by mixing the prepared ZnO nanoparticle solution with the Au nanoparticle solution as prepared in aforementioned sections. Firstly, 1 mL of Au nanoparticles solution is taken in a beaker with 10 mL DI water. After this, ZnO nanopowder (0.1 gm) is poured in the Au solution and the mixture is ultrasonicated at 44 kHz frequency (m/c: Sonics, Vibra cell) for 2 hours. The resultant mixture is then heated to 200ºC until the solution is completely dried. The dried particles are then collected in separate vials. This powder is taken with 1 mL of DI water and spread over the copper grid and dried for 24 hours beneath a 60-watt bulb. The prepared grid is then imaged with TEM. One can see the Au particles and the ZnO clusters placed side by side as should generally happen in the wet media self-assembly. Figure 2 (a), (b) below are the TEM images of the nanocomposite as obtained which are further utilized for doping onto the porous matrix of the organosilicate film. Figure 2(b) shows the side by side placement of the particle assembly. There are also certain areas which show the presence of core-shell architecture with the core being that of Au and the shell being the ZnO. The side by side orientation indicates that the local plasmon effect in Au clusters would happen due to the release of electrons from ZnO owing to the changed band gap may create a strong electric field which changes the overall emission frequency. With the use of aforementioned approach, metal-semiconductor interface has been developed which on an overall basis provides a band bending phenomenon changing the band gap value of this nanocomposite structure to be in between that of ZnO (~360 nm) and Au (550 nm). These values can be visualized in Figure 2 (d) where UV-vis spectra of ZnO-Au composite is shown.

After synthesizing ZnO-Au composite as mentioned, it is doped inside the nanoporous matrix by co-dissolution with the PMSSQ (polymethyl silsesquioxane) nanoparticles in the PGMEA (Propylene glycol monomethyl ether acetate) solution in an ultra-sonicator for 30 minutes. The porogen, PPG (polypropylene glycol) is then mixed in the solution which helps in self- assembling of the PMSSQ and ZnO-Au composite together while also generating the pores by self-volatilizing as studied earlier [Gupta et al., 2015]. After mixing of the ZnO-Au clusters with the PMSSQ, the solution becomes viscous and violet in color (Figure 2(c-a)). A thin layer of this viscous solution is then coated over the silicon (Si) substrate in thickness 5-10 ìm, controllable by spin speeds. The deposited film is then heated on a hot plate at 200ºC for 5 minutes; the PPG and PGMEA evaporate off leaving the complex network of PMSSQ and ZnO-Au linkages onto the Si surface, hence developing a nanoporous organosilicate (NPO) film. Figure 2 (c) shows how the color of the solution changes with every forward step, (a) shows the ZnO-Au doped NPO solution which is coated on the Si substrate, (b) shows ZnO-Au nanoparticle solution and (c) shows Au nanoparticle solution.

Figure 3 represents the characterization of the deposited film usingField Emission Scanning Electron Microscope (FESEM)(a) and Energy Dispersive Spectroscopy (EDAX) analysis (b).Table 1 presents the elemental composition as obtained through EDAX. The various peaks in the elemental map show presence of silicon, zinc, oxygen,and gold, all of them together which also endorses our FTIR plots of bondage between the core-shell clusters and the silica matrix (Figure 7). FTIR shows the -CH stretching vibration band (2800-300 cm^{-1}) which is due to the presence of propyl chain added with trimethoxysilane during surface silanization.

Table 1: Elemental composition as obtained through EDAX

Element	Weight %	Weight %, σ	Atomic %
Carbon	7.17	0.76	16.19
Oxygen	13.86	0.49	23.51
Silicon	55.87	0.85	53.97
Zinc	11.36	0.43	4.71
Gold	11.74	0.88	1.62

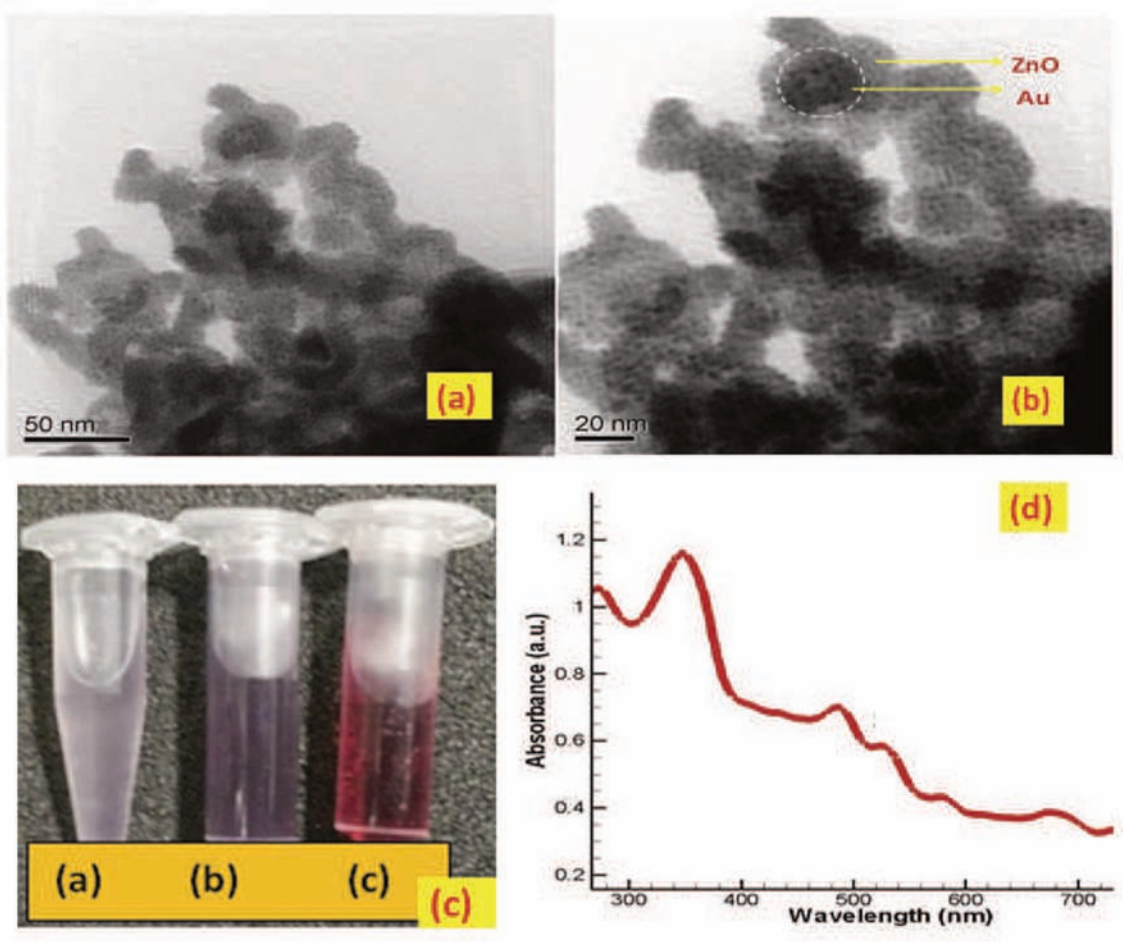

Figure 2: (a), (b) TEM images of ZnO-Au nanocomposite; (c) Nanoparticle solutions; (d) UV-vis spectra of ZnO-Au nanocomposite solution

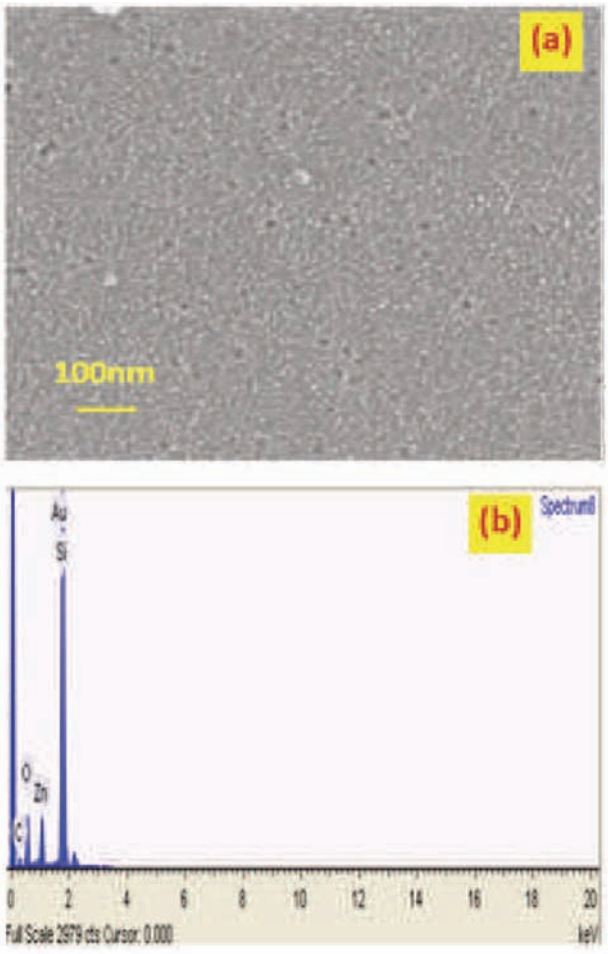

Figure 3: (a) FESEM image of ZnO-Au doped NPO film; (b) EDAX analysis

The absorbance spectra gave strong evidence about the successful alteration of the chemistry of silica film. Amide bands are clear from the spectra. Amide band is associated with C=O stretching vibration as well as N-H bending vibration and C-N stretching vibration. Peaks at 1580 $cm^{-1}$are mainly due to the R-NH_2 band. These results in the peak intensity with immobilized protein concentration in the material was observed.

Figure 4 represents the Raman spectra of all the fabricated constituents or the nanocomposites at 514 nm laser. The figure elaborates major peaks

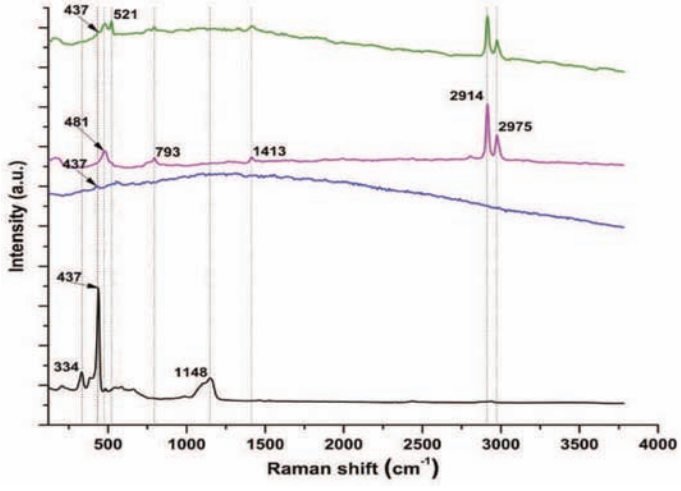

Figure 4: Raman spectra of various constituents/composites ZnO nanoparticles; ZnO-Au nanocomposite; NPO film; ZnO-Au doped NPO film

associated with the respective constituents and their composites. ZnO has shown major peaks around 334, 437 and 1148 cm^{-1}. The most significant peak amongst these peaks is around 437 cm^{-1}, which is representative of the E_2 mode wurtzite type phase of ZnO, while peak at 1148 cm^{-1} is representative of phonon vibrations of the ZnO structure and peak at 334 cm^{-1} is representative of the second order vibrational Raman mode due to multiple scattering as reported in the earlier literature as well [Chauhan et al., 2019]. ZnO-Au composite shows a small peak at 437 signifying ZnO in the composite. NPO film has shown major peaks at 481, 793, 2914 and 2975 cm^{-1}, where 481 cm^{-1} signifies symmetric stretching-bending mode due to the motion of O in Si-O-Si. The peak at 793 cm^{-1} signifies Si-O stretching [Cendrowski et al., 2011] while peaks at 2914 and 2975 cm^{-1} represent symmetric and asymmetric C-H vibrations [Kulkarni et al., 2008]. The Raman spectra of the ZnO-Au-NPO composite signifies the presence of various bonds and vibrations due to the various combinations.

3. Results and Discussion

3.1 Assessment of binding capability of novel ZnO-Au-NPO film with acridine orange dye and comparison with NPS film alone with fluorescence characterization

Before performing the fluorescence labeling test with protein-AF dyes and assessment of the immobilization of the fluorescent labeled antibody to perform FRET phenomenon over the fabricated film, we have tested our sensing platform with the acridine orange dye immobilization and quantized the fluorescence intensity. Acridine orange dye solution is poured over the developed film and incubated for 2 hours. The film is then washed with PBS buffer. After properly drying it, the image of the film is taken with the help of a fluorescence microscope in FITC filter mode. We have also shown a comparison of three differently coated platforms for their binding affinity to fluorescence and related species. The first film is simply NPO film (made at first attempt of this work), second is a ZnO doped NPO film and the third is a ZnO-Au doped NPO film. Fluorescent count of each response is calculated with the help of ImageJ software (Figure 5). Imaging data were acquired by an inverted fluorescence microscope over 6 places in a film. Mean of each data series along with an error bar is taken and the response is plotted against various films made. The response of the ZnO-Au doped NPO film is found to be greater than other films, which confirms the better fluorescence binding capability of novel "ZnO-Au" doped porous organosilicate film as compared to the ZnO-NPO and NPO films.

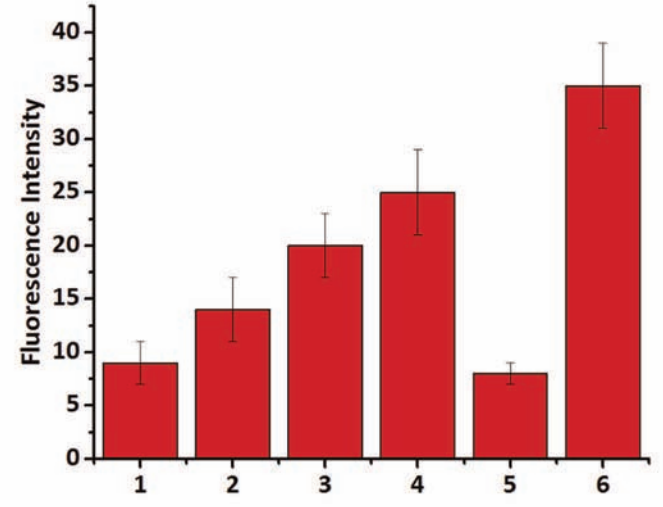

Figure 5: Fluorescence intensity with error bar on different samples, (1) NPO, (2) Dye-labeled NPO, (3) ZnO-NPO, (4) Dye-labeled ZnO-NPO, (5) Au-ZnO-NPO, (6) Dye-labeled Au-ZnO-NPO

3.2 Fluorescent spectra of Antibody-Acceptor fluorophore (Alexa Fluor 546) complex and Protein-G-donor fluorophore (Alexa Fluor 594) complex:

Biosensor response was measured by observing the intensity of the fluorescence peaks obtained from the spectrofluorometer scans. The fluorescence spectral responses of antibody (Ab) and AlexaFluor 546

(donor fluorophore) binding, Protein-G with AlexaFluor 594 (acceptor fluorophore) and combined spectral response (Ab-546 and PG-594 in mixed condition) are analyzed and plotted. Figure 6 (a) shows the response of fluorescence of the antibody recorded at an excitation wavelength of 540 nm which provides an emission peak at 571 nm. Figure 6 (b) shows the confirmation of fluorophore affinity with protein G. The plots represent that the donor Alexa Fluor 546 gets conjugated to antibodies as shown by red emboldened curve, while Alexa Fluor594 was conjugated to proteins G in a pink emboldened curve, as represented in Figure 6 (c). Figure 7 shows a comparison of the wavelength intensity shift plot in case the conjugation.

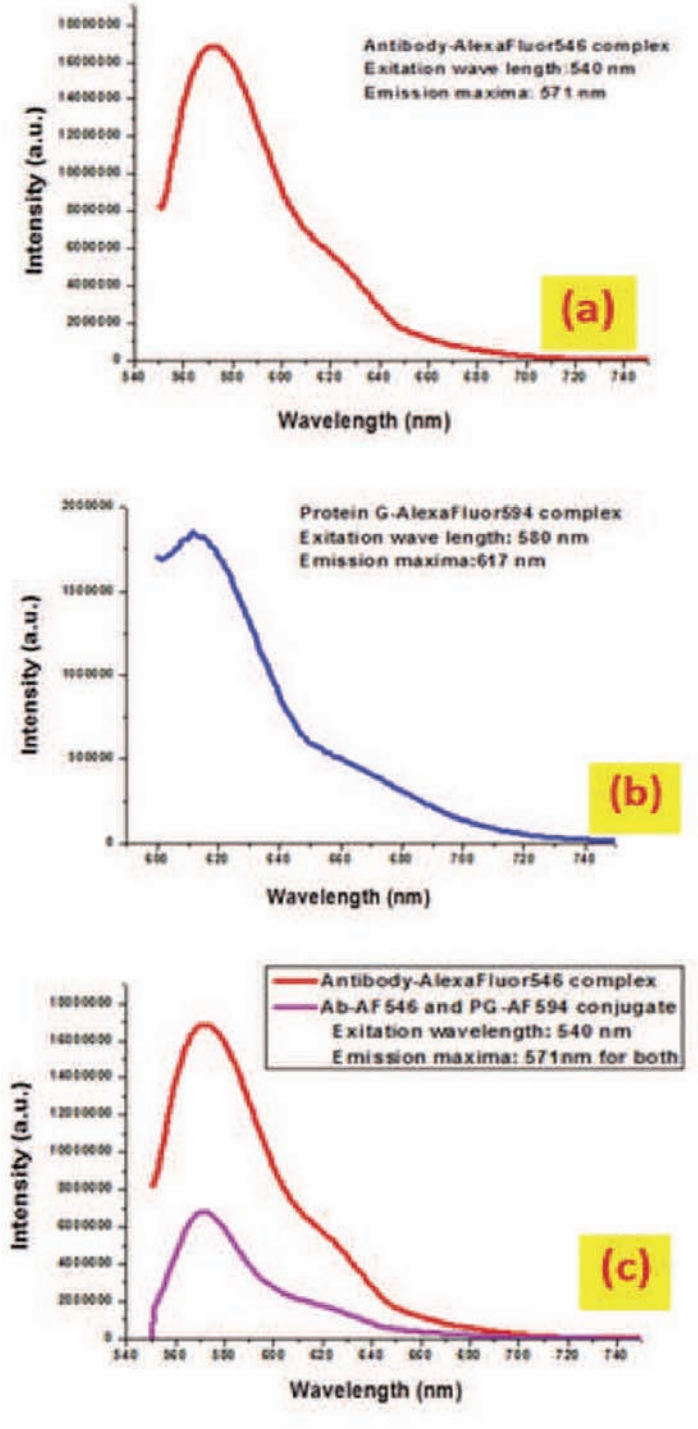

Figure 6: Fluorescence emission spectra of Antibody-Acceptor fluorophore (Alexa Fluor 546) complex and (b) Protein-G-donor fluorophore (Alexa Fluor 594) complex. (c) Represents the combined effect of antibody-AF546 and ProteinG-AF594.

The figure shows a significant intensity shift through the conjugation. Figure 8 depicts the FTIR response of the fabricated nanocomposite structure with protein-G and further antibody conjugation for 1 hr and 2 hr respectively.The FTIR curve represents that with the conjugation peaks have shown a different behavior. With the protein-G conjugation, the peaks at 1106 and 1646 have broadened, while after antibody conjugation the peaks have shown a different behavior. A significantly varied behavior can be observed with 1 hr conjugation and 2 hr conjugation, mainly along the 1000-1750 nm wavelength. The peak at 2347 has shown quite a consistent behavior with every conjugation step, protein conjugation, antibody conjugation and further incubation showing a broadening of the peak with every step.

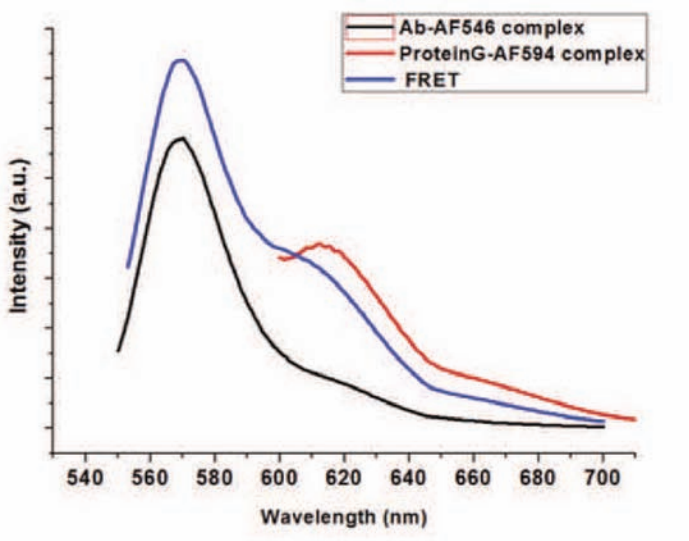

Figure 7: Wavelength shift during conjugation

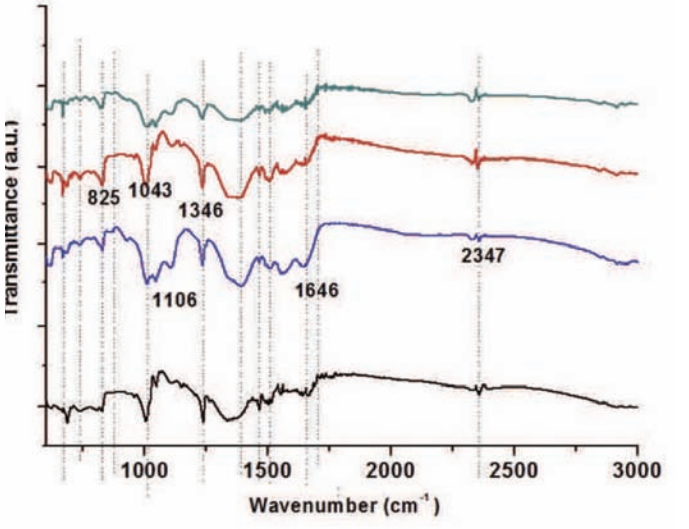

Figure 8: FTIR response for – ZnO-Au-NPO nanocomposite, – ZnO-Au-NPO-protein-G conjugation,– ZnO-Au-NPO- protein-G -Antibody (1 hr), –ZnO-Au-NPO- protein-G -Antibody (2 hr)

3.3 In solution FRET

Firstly FRET phenomenon is tested in solution. As it is well known that the optical biosensor response is a result of a larger number of conformational changes taking place in the sensor solution upon antigen binding. Figure 9(a) shows the schematic representation of the FRET mechanism with energy exchange with accepter-donor interaction.The schematic shows that the conformational changes alter the distance between the donor and acceptor, causing a measurable change in the resonance energy transfer that occurs between the fluorescent molecules. The result

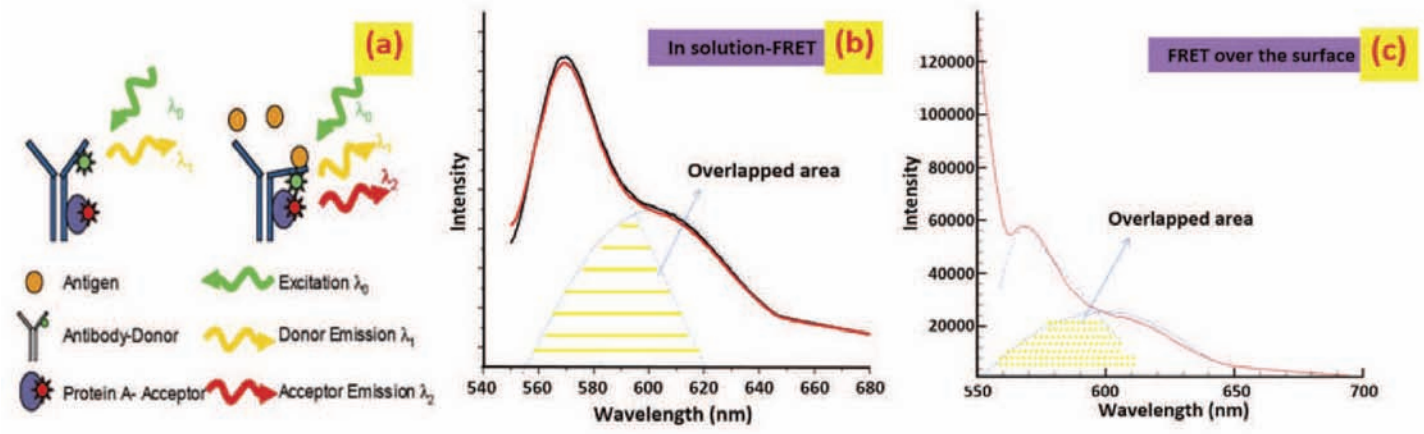

Figure 9: (a) The schematic representation of the FRET mechanism with energy exchange with accepter-donor interaction; (b) In solution FRET with *E. coli* antigen; 4 I antigen; 8 I antigen at an excitation wavelength of 540 nm; (c) FRET over ZnO-Au doped NPS film over the Si substrate.

is a derived measurement of antigen concentration in the solution based on changes in the observed spectral properties. Here, the conjugation of antibody to fluorophores and protein etc. and purification were conducted according to the protocol as mentioned above. Briefly, 25 µl monoclonal antibody, 10 µl sodium bicarbonate, and 65 µl PBS were combined and added to the Alexa Fluor 546 reactive fluorescent dye vial. The reaction mixture was incubated for 1 hour at room temperature. Figure 9 (b) shows in solution FRET with *E. coli* antigen at different concentration values.

It can be observed that as the *E. coli* were introduced, the labeled antibody/PG complex reduced the distance between the dye pairs due to the conformational change of antibody via antigen binding. As can be seen from the figure, the intensity peak gets suppressed (at ~610 nm) as antigen-antibody interaction takes place.

3.4 FRET test performed over the novel nanomaterial

Firstly, the films were silanized according to the aforementioned procedure. To immobilize the sensing elements, the films were incubated overnight at 4°C in the labeled antibody–protein G complex solution. This produced a sensing region on the surface of the film. The immobilization method is based on the covalent interaction between protein G and the film by means of the bifunctional crosslinkers bound to the silane film on the substrate surface. The labeled antibody–PG complexes were effectively immobilized on the film. Below is the FRET response when antigen 100 CFU/mL (4 µl *E. coli* solution) is taken for antibody reaction.

Figure 9 (c) depicts FRET phenomenon as happed over ZnO-Au doped NPO film over Si substrate. We have tested the fabricated platform for FRET to happen. Although the results showed are preliminary and several experiments need to be performed further in order to increase the FRET efficiency, but overlapped area shown in the above figure confirms the FRET.

4. Conclusions

In conclusion, we have fabricated a portable dipstick model based biosensor. The biosensor comprises a novel nanocomposite assembly (ZnO-Au-NPO) film, which can be utilized for fast sensing. Hence a coated flat chip is reported which can be envisioned as a dipstick model for the portable biosensor. The detection sensitivity as obtained in the present detection strategy is 100 CFU/mL, which can be further refined to approach 1 CFU/mL detection level.

Acknowledgments

The authors sincerely acknowledge the financial support from the Department of Biotechnology, India, Project No.: DBT /ME /20120130.

References

[1]Bhatt G, Bhattacharya S, 2018, DNA-Based Sensors. Environ. Chem. Med. Sensors, Springer

[2] Bhatt G, Kant R, Mishra K, Yadav K, Singh D, Gurunath R, Bhattacharya S,2017, Impact of surface roughness on Dielectrophoretically assisted concentration of microorganisms over PCB based platforms, Biomed Microdevices, 19, 28

[3] Bhattacharya S, Salamat S, Morisette D, Banada P, Akin D, Liu YS, et al., 2008, PCR-based detection in a micro-fabricated platform, Lab Chip, 8,1130

[3] Cendrowski K, Chen X, Zielinska B, Kalenczuk RJ, Rümmeli MH, Büchner B, et al., 2011, Synthesis, characterization, and photocatalytic properties of core/shell mesoporous silica nanospheres supporting nanocrystalline titania, J. Nanoparticle Res., 13, 5899–5908

[4] Chauhan PS, Kant R, Rai A, Gupta A, Bhattacharya S, 2019, Facile synthesis of ZnO/GO nanoflowers over Si substrate for improved photocatalytic decolorization of MB dye and industrial wastewater under solar irradiation. Mater Sci Semicond Process, 89, 6–17

[5] Foresman JB, Head-Gordon M, Pople JA, Frisch MJ, 1992, Toward a systematic molecular orbital theory for excited states, J Phys Chem, 96, 135–149

[6] Gupta A, Mondal K, Sharma A, Bhattacharya S, 2015, Superhydrophobic polymethylsilsesquioxane pinned one dimensional ZnO nanostructures for water remediation through photo-catalysis. RSC Adv, 5, 45897–45907

[7] Himcinschi C, Friedrich M, Murray C, Streiter I, Schulz SE, Gessner T, et al., 2001, Characterization of silica xerogel films by variable-angle spectroscopic ellipsometry and infrared spectroscopy, Semicond Sci Technol, 16, 806–811

[8] Kant R, Bhatt G, Sundriyal P, Bhattacharya S, 2017, Relevance of Adhesion in Fabrication of Microarrays in Clinical Diagnostics. In: Mittal KL, Etzler FM, editors. Adhes. Pharm. Biomed. Dent. Fields, Scrivener Publishing LLC, 257–298

[9]Korampally V, Yun M, Rajagopalan T, Dasgupta PK, Gangopadhyay K, Gangopadhyay S, 2009, Entropy driven spontaneous formation of highly porous films from polymer-nanoparticle composites, Nanotechnology,20

[10] Kulkarni MM, Bandyopadhyaya R, Sharma A, 2008, Janus silica film with hydrophobic and hydrophilic surfaces grown at an oil-water interface, J Mater Chem, 18, 1021–1028

[11] Luo X, Morrin A, Killard AJ, Smyth MR, 2006, Application of nanoparticles in electrochemical sensors and biosensors, Electroanalysis, 18, 319–326

[12] Nayak M, Singh D, Singh H, Kant R, Gupta A, Pandey SS, et al., 2013, Integrated sorting, concentration and real time PCR based detection system for sensitive detection of microorganisms, Sci Rep, 3, 3266

[13] Rim YS, Bae SH, Chen H, De Marco N, Yang Y, 2016, Recent Progress in Materials and Devices toward Printable and Flexible Sensors, Adv Mater, 28, 4415–4440

[14] Scandale W, Efthymiopoulos I, Still DA, Carnera A, Della Mea G, De Salvador D, et al., 2008, Apparatus to study crystal channeling and volume reflection phenomena at the SPS H8 beamline, Rev Sci Instrum, 2008

[15] Seidel H, 1990, Anisotropic Etching of Crystalline Silicon in Alkaline Solutions, J Electrochem Soc, 137, 3612

[16] Su HW, Chen WC, 2009, Preparation of nanoporous poly(methyl silsesquioxane) films using core-shell silsesquioxane as porogen, Mater Chem Phys, 114, 736–741

[17] Uttamchandani M, Neo JL, Ong BNZ, Moochhala S, 2009, Applications of microarrays in pathogen detection and biodefence, Trends Biotechnol, 27, 53–61

[18] Wang J, 2005, Carbon-nanotube based electrochemical biosensors: A review, Electroanalysis, 17, 7–14